

Effective Methylene Dye Removal from Contaminated Water using Zinc Oxide Nanoparticles Fabricated from the Green Synthesis of *Laurus nobilis* Leaf

^{1,2}Doga Kavaz

¹Department of Bioengineering, ²Environmental Research Center Cyprus International University, Nicosia, Mersin 10 Turkey.

dkavaz@ciu.edu.tr

(Received on 28th December 2023, accepted in revised form 22nd July 2024)

Summary: Methylene blue (MB), a prevalent pollutant in textile industry wastewater, poses significant environmental and health risks due to its toxicity, mutagenicity, and persistence. Effective remediation strategies are essential for mitigating its impact. This study presents a novel approach using Zinc Oxide (ZnO) nanoparticles synthesized via a green synthesis method employing *Laurus nobilis* leaf extract. This environmentally friendly method avoids harmful chemicals and enhances the safety of nanoparticle disposal. The ZnO nanoparticles, characterized by X-ray diffraction (XRD), scanning electron microscopy (SEM), and Fourier-transform infrared spectroscopy (FTIR), were monodispersed with an average size of 68.5 nm and showed excellent morphological properties. The nanoparticles achieved a maximum dye removal efficiency of 99% under optimal conditions of pH 3 and a contact time of 150 minutes. The maximum adsorption capacity of the ZnO nanoparticles for MB was 33.75 mg/g. The adsorption kinetics and isotherms were effectively described by the pseudo-second-order kinetic model and both the Freundlich and Langmuir adsorption models, with the Langmuir model indicating a monolayer adsorption capacity of 30.98 mg/g. The correlation coefficients (R^2) for the Langmuir and Freundlich models were 0.9421 and 0.9463, respectively, demonstrating the robustness of these models in describing the adsorption behaviour. This study not only underscores the potential of green synthesized ZnO as an effective adsorbent for dye remediation but also contributes significantly to sustainable practices in environmental management.

Keywords: Methylene Blue, Nanoparticle, Contaminated water, Green synthesis, Morphological characteristics.

Introduction

The widespread use of organic dyes in global industries poses a significant threat to environmental and human health. Industries such as textiles, plastics, cosmetics, and printing extensively employ mutagenic, carcinogenic, and allergenic organic dyes for colouration purposes [1]. The discharge of these complex aromatic structures into water bodies without adequate purification has led to a critical environmental issue, particularly impacting aquatic ecosystems [2], necessitating innovative and sustainable strategies for their removal from industrial wastewater. Traditional methods, including chemical coagulation, adsorption, and advanced oxidation processes, have exhibited limitations such as high operational costs, the generation of toxic by-products, and inefficiencies in achieving complete dye removal [3].

Methylene blue (MB), with its complex heterocyclic aromatic structure and inherent resistance to degradation, emerges as a persistent pollutant in wastewater [4]. Its distinctive deep blue colour, broad absorption spectrum, and solubility make it a versatile dye for applications ranging from staining biological tissues to serving as an indicator in chemical reactions

[6]. However, the widespread use of MB poses significant environmental challenges when these compounds contaminate water bodies. In industrial processes, especially within the textile sector, MB is extensively utilized to impart vibrant blue hues to fabrics [7]. The discharge of wastewater containing MB, often without proper treatment, contributes to water pollution. The potential toxicity, mutagenicity, and persistence of MB in aquatic ecosystems underscore the urgent need for effective remediation strategies to mitigate its impact on environmental and human health [8]. The dye's remarkable versatility in industrial applications, coupled with its resistance to conventional treatment methods, further underscores the critical need for advanced remediation technologies [9].

Adsorption techniques utilizing various materials, such as activated carbon, zeolites, and clay minerals, have emerged as promising solutions for the removal of coloured dyes from wastewater [10]. While these adsorbents offer advantages such as high adsorption capacities and ease of regeneration, their susceptibility to fouling, the need for frequent regeneration, and challenges in scaling up for

*To whom all correspondence should be addressed.

industrial applications necessitate the exploration of alternative materials [11]. Nanoparticles, owing to their unique physicochemical properties arising from their nanoscale dimensions, have emerged as promising entities for various environmental applications, particularly wastewater treatment [12]. In the context of dye removal from industrial effluents, nanoparticles exhibit distinct advantages over conventional methods. Their high surface area-to-volume ratio, enhanced reactivity, and tunable surface functionalities make them exceptionally effective in adsorbing, degrading, or immobilizing dye molecules, thereby offering a novel approach to address the challenges associated with dye pollution in water bodies [13]. Among nanoparticle categories, metal oxide nanoparticles stand out for their exceptional capabilities in dye removal. Metal oxide nanoparticles, with their exceptional physicochemical properties, present an innovative avenue for overcoming the limitations associated with traditional adsorbents [14]. Several works have investigated the utilization of treating dye-contaminated wastewater. The work of [15] carried out a green synthesis approach to make Zinc Oxide nanoparticles from an Indian Tulsi leaf. Their investigation involved the removal of Congo red dye from dye-contaminated water. Their research validated the higher efficiency of biosynthesized as compared to commercially available (chemically synthesized) nanoparticles. Their result showed the maximum Congo red removal was 97% at optimum conditions of pH of 4 and contact time of 30 minutes. The photocatalytic degradation of MB dye using a nanocomposite of Titanium Oxide/Graphene Oxide (TiO_2/GO) was investigated in the work of [8]. Their result showed that at a weight ratio of 1:2 TiO_2/GO , the maximum MB removal (99%) was achieved, as against 30% MB removal using TiO_2 . The maximum MB removal was achieved at conditions of pH of 10, and 0.2 g/L adsorbent dose. The removal of Cationic dye using fabricated nano-alumina was investigated in the work of [16]. In their study, a maximum dye removal of 100% was achieved at optimum conditions of pH=4, contact time of 120 minutes, and adsorbent dosage of 5 mg/mL. Their result also showed that the adsorption capacity of the Cationic dye (Rhodamine B) on the nano-alumina was 165 mg/g.

Characterized by high surface area and reactivity, metal oxide nanoparticles have been extensively investigated for their efficacy in wastewater treatment. These nanoparticles demonstrate a remarkable ability to adsorb dye molecules, providing a compelling alternative to traditional adsorbents. The tunable surface functionalities of metal oxide nanoparticles enable customization for specific dye types, enhancing their

selectivity and efficiency in complex wastewater matrices. The work by [18] used the co-precipitation method to synthesize the Iron-Oxide (Fe_3O_4) nanoparticles loaded activated carbon (AC) for adsorption experiments. Their work demonstrated that the synthesized nanoparticle achieved maximum removal of the methylene blue dye and green dyes of 138mg/g and 166.6 mg/g respectively. The removal of both cationic and anionic dyes using synthesized Zinc Oxide (ZnO) was investigated in the work of [19]. In their study, the maximum adsorption capacity for the acid fuchsin and Congo Red, which are the anionic dyes was 3307 and 1554 mg/g respectively, while the maximum adsorption for the malachite green (cationic dye) was 2963 mg/g. Their work conclusively stated that the ZnO nanoparticle could be reused several times without losing its adsorption ability.

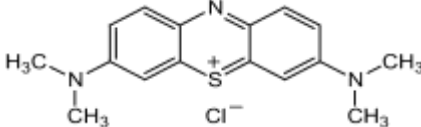
ZnO nanoparticles are effective for dye removal in wastewater due to their biocompatibility, stability, and photocatalytic activity. Conventional chemical synthesis methods for these nanoparticles are environmentally harmful, involving hazardous chemicals, high temperatures, and energy-intensive processes, leading to toxic by-products and increased greenhouse gas emissions. Additionally, these methods are costly and rely on non-renewable resources.

To address these issues, biosynthesized nanoparticles using natural sources like plant extracts offer a sustainable alternative. This green chemistry approach provides an eco-friendly and efficient solution for wastewater treatment, enhancing the removal of dyes without the environmental drawbacks of conventional methods.

Some researchers have considered the synthesis of ZnO using the green synthesis method. In the work by [20], their study presents the synthesis of ZnO nanoparticles using a green process with *Agathosma betulina* extract. The nanoparticles, averaging 15.8 nm, were analyzed using various spectroscopy and microscopy techniques. A pellet made from these nanoparticles showed a notable nonlinear current-voltage response, characteristic of a varistor. In a similar work by [21], their study reports the green biosynthesis of ZnO nanoparticles using *Solanum nigrum* as a capping agent. The nanoparticles, with an average size of 20-30 nm, were characterized using various techniques, including UV-Vis DRS, PL, XRD, FTIR, FE-SEM, TEM, TG-DTA, and XPS. Key findings include an indirect band gap of 3.38 eV, blue and green photoluminescence emissions, and a wurtzite hexagonal structure. The FTIR spectra indicated proteins as stabilizing agents. The

nanoparticles demonstrated significant antibacterial activity, suggesting potential applications in medical and industrial fields. Likewise the work by [22], their study evaluates Hibiscus sabdariffa flower extracts' effect on green synthesis of ZnO for photocatalytic degradation of methylene blue (MB). Using zinc nitrate, extracts of 1%, 4%, and 8% served as reducing and stabilizing agents. FTIR showed a Zn-O bond at 618 cm^{-1} , XRD confirmed a hexagonal Wurtzite phase, and XPS indicated Zn^{+2} states. Nanoparticle sizes ranged from 8 to 30 nm, with band gaps decreasing from 2.96 to 2.77 eV as extract concentration increased. The ZnO nanoparticles degraded 97% of MB in 150 minutes, demonstrating high photocatalytic efficiency. This research introduces a pioneering paradigm by focusing on the utilization of ZnO nanoparticles synthesized from *Laurus nobilis* leaves for the removal of MB dye (See Properties in Table 1). The green synthesized nanoparticles inherit the unique properties of ZnO, adding an innovative dimension to the conventional synthesis methods. The integration of green synthesis aligns with the principles of environmental sustainability, avoiding the use of harsh chemicals and promoting a sustainable approach to nanoparticle production. This study aims to evaluate the efficiency of *Laurus nobilis*-derived ZnO nanoparticles in removing MB dye from aqueous solutions, offering a sustainable solution to the challenges associated with organic dye pollution. The outcomes of this research contribute not only to the field of wastewater treatment but also pave the way for the development of sustainable nanomaterials for broader environmental applications.

Table-1: Properties of MB [23].

Chemical Structure	
	
pH	Basic
Colour	MB gives off a dark green colour in solid form at room temperature. When dissolved in water, it yields a blue solution
Odor	MB is Odorless
Solubility	35%
Physical State at room temperature	Solid
Chemical formula	$\text{C}_{16}\text{H}_{18}\text{N}_3\text{ClS}$
Molecular Mass (g/mol)	319.85

Experimental

Materials

Both the zinc acetate dihydrate ($\text{Zn}(\text{CH}_3\text{CO}_2)_2 \cdot 2\text{H}_2\text{O}$) and the sodium hydroxide (NaOH)

used for this study were acquired from Sigma Aldrich and used in their unpurified forms. To dilute the solutions, de-ionized water was used.

Aqueous Leaf Extract Preparation

The *Laurus nobilis* leaves were cleaned with water from the tap and then with deionized water to purify them from dust and foreign wastes and dried by laying in the shade at ambient temperature. The extract was prepared by grinding dried bay leaves into a powder and then sieving the powder using particle size of 0.630 – 1.00 mm to remove any larger particles. In a 250 ml flask, we cooked 2.5 g of powdered bay leaves with deionized water, 100 ml under reflux for five minutes. The extracted liquid was allowed to cool at ambient temperature before being filtered. To get rid of any lingering plant material or contaminants, the extract was centrifuged at 9500 rpm for 5 minutes before being stocked at 4°C .

The function of *Laurus nobilis* leaf extract is to provide chemicals that aid in the stabilization and reduction of ZnO nanoparticles in a natural and environmentally friendly manner. Bay leaves, or *Laurus nobilis*, contain several bioactive compounds, including terpenoids, flavonoids, and polyphenols, which have reducing and capping effects. The leaf extract functions as a reducing agent, giving the metal ions (like zinc ions) the electrons, they need to become the matching nanoparticles. The creation of ZnO nanoparticles is made possible by this reduction process. By interacting with the metal ions and encouraging their transformation into nanoparticles, the bioactive substances found in the *Laurus nobilis* extract are essential to this reduction process. The *Laurus nobilis* leaf extract also functions as a stabilizer, inhibiting the aggregation or agglomeration of the synthesized nanoparticles. The bioactive substances in the extract can attach to the nanoparticles' surfaces and create a barrier that prevents particle-particle interactions. The ZnO nanoparticles in the synthesized fluid are stabilized and kept dispersed by this stabilizing effect. We used a green and sustainable strategy by using *Laurus nobilis* leaf extract in the synthesis process instead of harmful chemicals or solvents. For the creation of ZnO nanoparticles, the extract offers a natural and friendly environment, making them appropriate for a variety of biomedical applications.

Nanoparticle Zinc Oxide Synthesis.

ZnO NP synthesis requires the use of zinc acetate dihydrate ($\text{Zn}(\text{CH}_3\text{CO}_2)_2 \cdot 2\text{H}_2\text{O}$) as a metal precursor. To synthesize ZnO nanoparticles, begin by

dissolving zinc acetate dihydrate ($\text{Zn}(\text{CH}_3\text{CO}_2)_2 \cdot 2\text{H}_2\text{O}$) in deionized water to prepare a 0.02 M solution. Separately, prepare an extract from *Laurus nobilis* leaves. Mix 10 ml of the *Laurus nobilis* extract with 90 ml of the zinc acetate solution at room temperature using a magnetic stirrer, and stir the mixture for two hours at ambient temperature. After stirring, adjust the pH of the mixture to 12 by adding 1 M NaOH drop by drop. Following pH adjustment, centrifuge the resulting white liquid at 9500 rpm for 30 minutes to separate the precipitate. Wash the obtained precipitate thoroughly with deionized water and ethanol to remove any impurities.

The resultant white-colored precipitate is then dried at 60°C overnight. This drying step is crucial as it removes any residual solvents, such as water or ethanol, used during the washing steps. This ensures that the nanoparticles are free from any contaminants that could affect their properties. The temperature is kept moderate to prevent any premature decomposition or structural changes in the nanoparticles. The drying process is carried out overnight to ensure thorough removal of solvents.

Following the drying process, the precipitate is calcined at 200°C for three hours. Calcination is a thermal treatment process used to further purify the nanoparticles and enhance their crystallinity. This step helps to remove any organic residues from the plant extract and to achieve the desired crystal structure of ZnO. The dried precipitate is heated in a furnace at 200°C for three hours. This temperature is sufficient to induce the formation of the crystalline phase of ZnO without causing excessive particle growth. The duration ensures complete transformation of the material into a stable and pure crystalline form.

These steps are crucial for obtaining high-quality ZnO nanoparticles with consistent size, shape, and properties, which are essential for their effectiveness in applications such as dye removal from contaminated water.

Analysis or Characterization of Synthesized Nanoparticles

UV-Vis spectroscopy

Synthesized ZnO NPs have their optical characteristics examined by UV-VIS spectroscopy. A spectrophotometer (Japanese-made Shimadzu 1800) was used to conduct an ultraviolet-visible

spectroscopic assessment. The wavelength range of the UV-visible spectrophotometer was 200–800 nm.

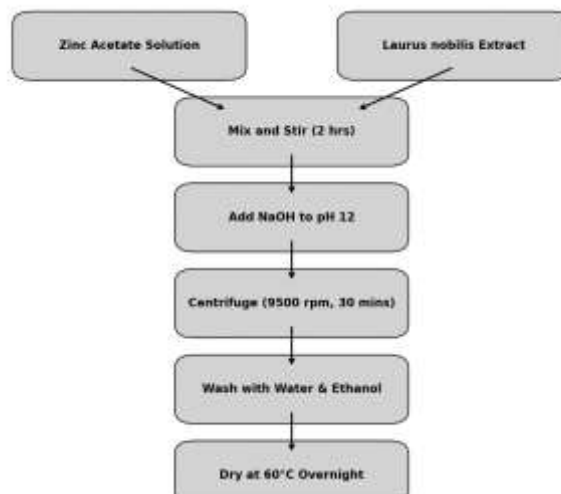


Fig. 1: Schematic diagram of ZnO synthesis.

Analysis Via X-Ray Diffraction (XRD)

High-resolution X-ray diffraction (XRD) patterns were generated using a Bruker D8 Advance diffractometer outfitted with a Cu X-ray tube and an incident beam Ge (111) monochromator (= 0.154056 nm).

Analysis via Scanning Electron Microscope (SEM)

Using a sputter-coated copper stub and 25 μL of the sample at 10 kV ultra-high resolution, freeze-dried pure ZnO NPs were analyzed for composition and structure, and images of ZnO NPs were analyzed with an FEI QUANTA-200 SEM. The image showed that the nanoparticles were spread out with minimal clustering.

FTIR Analysis (Fourier Transform infrared spectroscopy)

The zinc oxide nanoparticles' FTIR analysis was performed using a Perkin Elmer Spectrum RX1 (Range 400-4000 cm^{-1}).

Adsorption experiment

The dye adsorption experiments were conducted through the homogenous mixing of ZnO in MB dye solutions contained in a 250 mL beaker. Optimization of experimental variables encompassed the variations of dye concentration, pH, adsorbent dose, and contact time. Specifically, adsorption

experiments were executed using a 100 mL solution containing 0.2 mg/mL of Methylene Blue (MB) in a 250 mL Erlenmeyer flask. The experiments were carried out at room temperature (25 ± 1 °C) on an orbital shaker operating at a speed of 200 rpm. Monitoring of the absorbance changes in all solution samples occurred at predetermined time intervals throughout the adsorption process.

The adsorbent dose varied within the range of 0.05 g to 0.25 g/mL, and the dye concentration spanned from 10 mg/L to 90 mg/L. The mixing time was systematically adjusted from 5 minutes to 150 minutes, while the solution pH was modulated from 2 to 10 using a 0.01M solution of HCl or NaOH. Solution pH levels were accurately measured using a pH meter (Eutech Instruments, Singapore). Quantification of dye concentration was performed using a UV-VIS spectrophotometer.

The quantification of dye removal percentage and adsorption capacity was achieved through the utilization of the following equations.

$$\text{Dye removal (\%)} = \frac{(C_o - C_e)}{C_o} \times 100 \quad (1)$$

$$\text{Adsorption capacity } (q_e) = \frac{(C_o - C_e)V}{m} \quad (2)$$

where the mass of the ZnO nanoparticle is represented by m , the initial dye concentration is represented by C_o , C_e represents the equilibrium dye concentration in

mg/L, while the V in L represents the volume of the dye solution.

Results and Discussions

UV-Visible Spectroscopy Study

This research used a UV-vis spectrophotometer to successfully synthesize ZnO NPs from *Laurus nobilis* leaves extract across a 200-800 nm wavelength range with a 1 nm resolution. The UV-visible assessment was first utilized to examine the progress of produced Zinc Oxide NPs as they formed. Fig. 1 shows the UV-visible spectra of Zinc Oxide nanoparticles synthesized in *Laurus nobilis* leaves extract; ZnO NPs' SPR absorption is characterized by an absorption peak at 389 nm. ZnO NPs absorbance spectra were also measured between 350 and 390 nm, as reported by [24]. The size, average diameter, and shape of the nanoparticles all play a part in the structure of the plasmon band and the wavelength range in which it is seen [25]. It is well established that the UV-visible spectrum plasmon band gaps of ZnO NPs widen as the particles get smaller. For instance, The outcome of calcination temperature on the size of synthesized Zinc Oxide NPs was investigated by [26] observed that the plasmon band in the UV-visible spectrum of Zinc Oxide nanoparticles varies in intensity depending on the size of the particles [26]. The band gap was evaluated using the Tauc relation. The values estimated from the tauc relation are 2.89 eV. This is similar to the values retrieved in the literature[22].

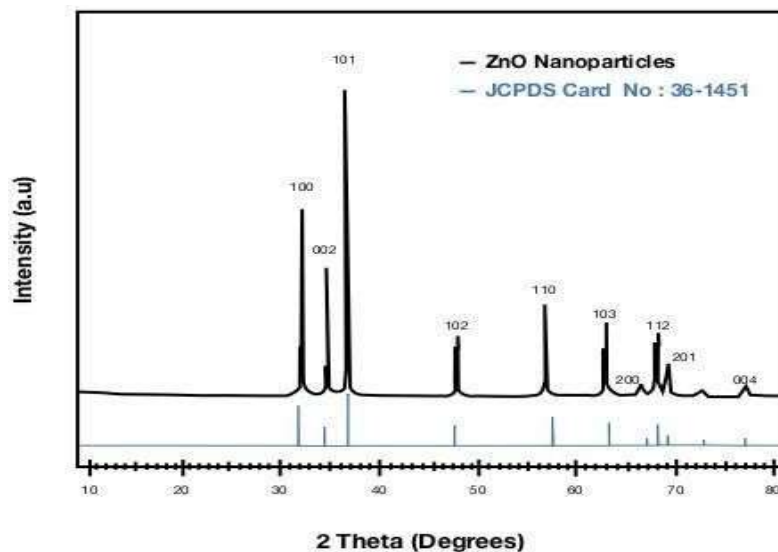


Fig. 1: UV-Visible spectrum of *Laurus nobilis* leaves' aqueous extract.

Analysis by X-Ray Diffraction (XRD)

After synthesis, the crystal structure of the Zinc Oxide NPs was determined by using XRD analysis. The ZnO NPs samples XRD patterns are presented in the ZnO hexagonal wurtzite phase (JCPDS file no. 89-7102) after calcination at 350 °Celsius, diffraction peaks were seen at (31.71), (34.31), (36.31), (47.51), (56.51), (62.81), (66.31), (67.91), (69.01), and (72.61). After synthesis, the crystal structure of the Zinc Oxide (ZnO) nanoparticles (NPs) was determined by using X-ray diffraction (XRD) analysis. The XRD patterns of the ZnO NP samples are presented in the ZnO hexagonal wurtzite phase (JCPDS file no. 89-7102) after calcination at 350°Celsius. The diffraction peaks were observed at 2θ values of 31.71°, 34.31°, 36.31°, 47.51°, 56.51°, 62.81°, 66.31°, 67.91°, 69.01°, and 72.61°. These peaks correspond to the diffraction lattice planes (100), (002), (101), (102), (110), (103), (200), (112), (201), and (004), respectively, as labelled in Fig. 2. The intensity values of the diffraction peaks in the XRD pattern provide information about the crystallinity and phase purity of the ZnO NPs. Higher intensity peaks indicate a higher degree of crystallinity. The relative intensities of the observed peaks are as follows:

- The peak at 36.31° corresponding to the (101) plane is the most intense, indicating that this is the

predominant crystallographic orientation in the sample.

- Peaks at 31.71° and 34.31°, corresponding to the (100) and (002) planes, also show significant intensity, suggesting that these orientations are also prominent in the ZnO NPs.
- The remaining peaks at 47.51°, 56.51°, 62.81°, 66.31°, 67.91°, 69.01°, and 72.61° have relatively lower intensities, indicating lesser but still notable crystallographic orientations within the ZnO NPs.

These intensity values are consistent with the standard diffraction pattern for ZnO wurtzite structure, confirming the successful synthesis of ZnO NPs with high crystallinity and phase purity. The dominance of specific peaks also indicates a preferential orientation, which could be attributed to the synthesis conditions and calcination process.

Following the ZnO hexagonal wurtzite structure according to the (JCPDS-36-1451), developed by the Joint Committee on Powder Diffraction Standards, the synthesised ZnO NPs exhibit characteristic XRD peaks. In the XRD study, just the characteristic diffraction peak for ZnO was seen, showing that the ZnO NPs did not contain any other contaminants. Some investigations have shown comparable findings [26]–[28]

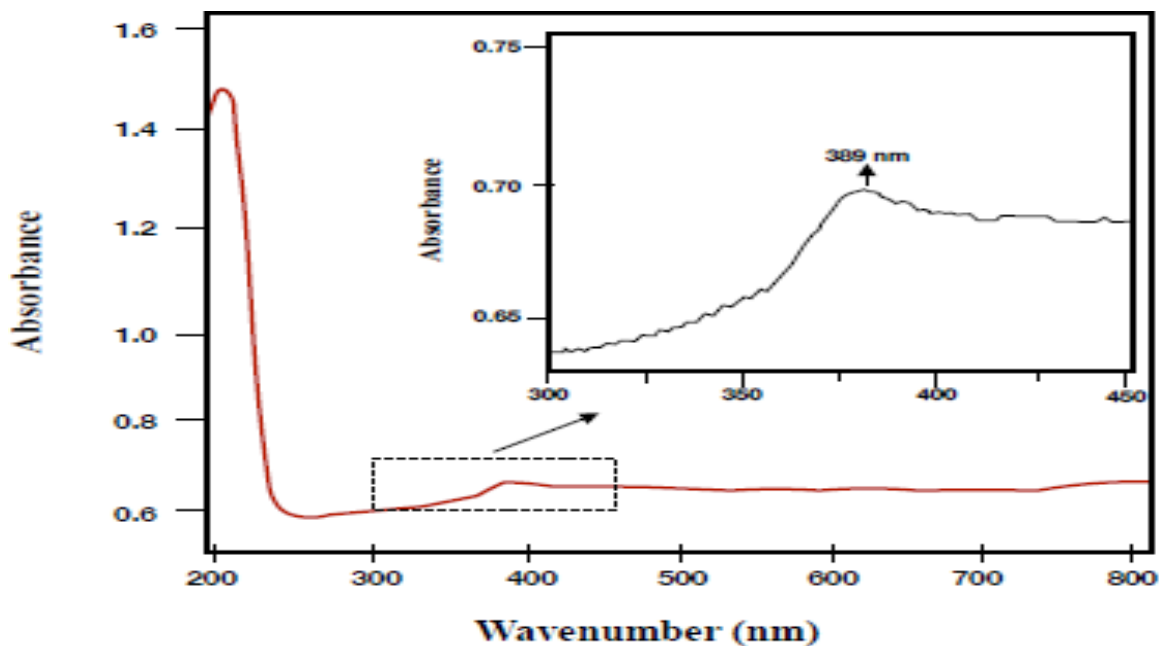


Fig. 2: XRD patterns of ZnO NPs.

Fourier Transform Infrared Spectroscopic Study

Fig. 3 displays the FTIR spectrum measuring synthesized ZnO nanoparticles (NPs) in the range of 500-4000 cm^{-1} . The bonding within the nanoparticles is confirmed by the pronounced vibration bands between 400 cm^{-1} and 500 cm^{-1} , which are characteristic features of Zn-O stretching vibrations.

Typically attributed to O-H stretching vibrations, a significant peak at 3450 cm^{-1} indicates the existence of hydroxyl groups. These could potentially signify the presence of water bound to the surface, hydroxyl groups intrinsic to the ZnO lattice, or moisture absorbed from the atmosphere. The peaks at 2900 cm^{-1} and 2430 cm^{-1} , often absent in pure ZnO, may indicate the presence of carbonaceous residues or organic contaminants on the nanoparticle surface, potentially originating from the synthesis procedure or handling.

The pronounced absorption features observed at 1450 cm^{-1} and 1653 cm^{-1} are attributed to water bending vibrations (H-O-H bending), providing additional evidence for the existence of moisture. The peak at 1356 cm^{-1} , when present, is typically associated with C-H bending vibrations, suggesting possible organic contaminants or residues from the synthesis process.

The peaks in the range of 500 cm^{-1} to 1200 cm^{-1} should be highlighted and explained. The peaks at 490 cm^{-1} and 450 cm^{-1} are characteristic of Zn-O stretching vibrations, confirming the presence of zinc oxide bonds in the nanoparticles.

In conclusion, based on the aforementioned observations, established data, and prior research, it can be deduced that the ZnO nanoparticles display not only the anticipated metal-oxide properties but also signs of surface-adsorbed species, including moisture and possible organic compounds.

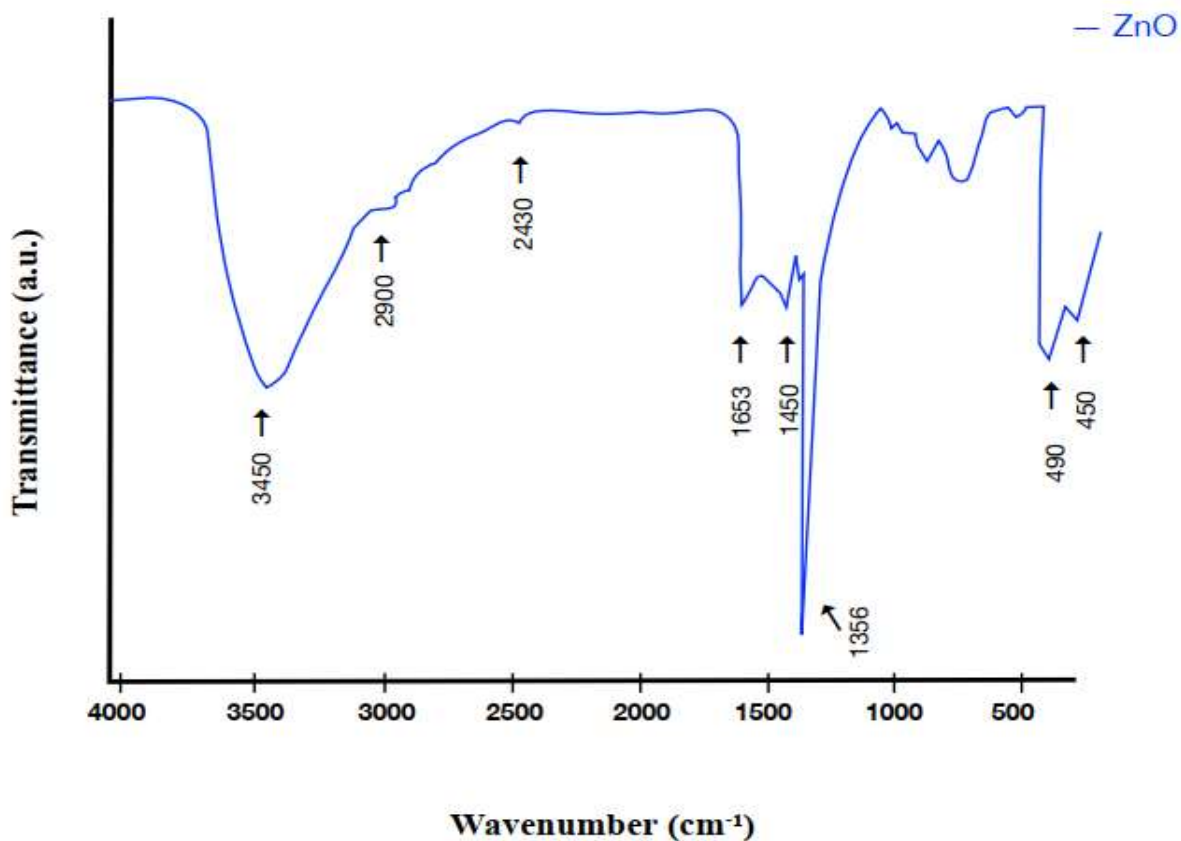


Fig. 3. FTIR spectrum for ZnO NPs.

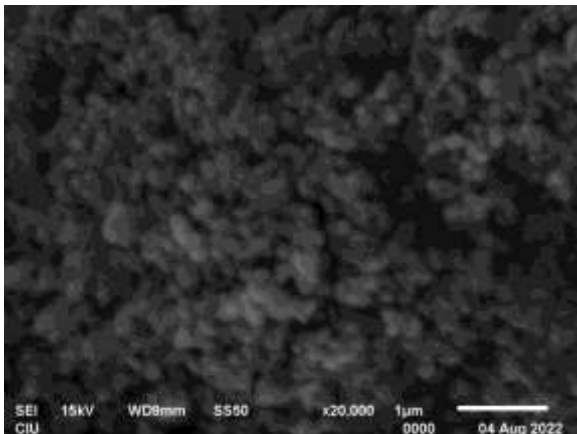


Fig. 4: SEM analysis of ZnO NPs.

Dynamic Light Scattering (DLS) Study

Average sizes of *Laurus nobilis*-mediated Zinc Oxide NPs were identified using the (DLS) experiments. ZnO nanoparticles averaged a diameter of 68.5 nm. The results of the analysis showed that the synthesized particles were ultrafine, having sizes of less than 100 nm. This provides solid evidence that *Laurus nobilis* extract successfully synthesized smaller NPs. One possible explanation is that it contains a greater variety of phytochemicals. Additionally, DLS analysis showed that the produced nanoparticles possessed very well-defined dimensions. NPs' antibacterial effectiveness increases with increasing size, with smaller NPs having greater surface area. The membranes of bacteria typically measure in the nanometer range. If these nanoparticles are lower in size than the cell membrane's pores, they have a better chance of penetrating the membrane and inhibiting bacterial growth.

Fig 4 shows leaf extract-derived ZnO nanoparticles in SEM. A topographical evaluation reveals that nanoparticles are often sphere-shaped, clustered, and have a rough surface. Additionally, SEM scans showed that plant-derived NPs are 100% pure, supporting the view that plants are incredibly capable of making ZnO NPs. The morphology of NPs is a crucial factor in their efficacy against infections. ZnO NPs synthesized from plants can be incredibly valuable when treating illnesses due to the spherical nature of the NPs, which makes them particularly effective during antibacterial activity by penetrating the cell wall of pathogens.

Effect of Experimental Conditions on Adsorption of MB Dye

Effect of Initial dye Concentration on Adsorption efficiency

The effect of the initial dye concentration on the adsorption efficiency was investigated experimentally from 10 mg/L to 90 mg/L (in increments of 10 mg/L). The mass of adsorbent added to each dye sample was 0.2 mg/mL, and the mixture was stirred at 200 rpm for 60 minutes. This was done at a controlled room temperature of 25 °C, and pH of 6. In Fig 5, we see that the adsorption capacity increases steadily with an increase in the dye concentration. At low concentrations between 10-40 mg/L, the percentage increase in the adsorption capacity is 74.2 %, whereas the percentage increase is 33.3 % between 50 mg/L and 90 mg/L. The observed trend, where the removal efficiency decreases with increasing dye concentration, can be explained by the availability of active adsorption sites on the ZnO nanoparticles. ZnO nanoparticles, especially those synthesized from natural materials like *Laurus nobilis* leaves, typically have a large surface area with numerous active sites for adsorption.

At lower dye concentrations (10-40 mg/L), there are relatively few dye molecules in the solution. Consequently, a greater proportion of the available active sites on the ZnO nanoparticles are accessible for adsorption. This leads to a higher percentage of dye molecules being adsorbed onto the nanoparticles, resulting in a high removal efficiency. Each dye molecule has ample active sites to adhere to, maximizing the removal efficiency. As the initial dye concentration increases (50-90 mg/L), the number of dye molecules in the solution rises significantly. Although the total adsorption capacity of the ZnO nanoparticles increases, the number of available active sites per dye molecule decreases. This results in a lower proportion of dye molecules being adsorbed onto the nanoparticles, reducing the removal efficiency. In essence, the active sites become saturated more quickly, and not all dye molecules find available sites for adsorption. The adsorbent dosage remains constant in this study, which means the number of active sites available for adsorption does not change. Therefore, at higher dye concentrations, the competition for available adsorption sites increases, leading to a decrease in the overall removal efficiency. This explains why the percentage of dye removal is higher at lower concentrations and decreases as the dye concentration increases, despite the constant amount of ZnO nanoparticles used as the adsorbent.

The higher adsorption capacity at low concentrations shows the high efficiency of green synthesized ZnO to remove MB from contaminated water. We also see a reduction in the removal efficiency with increasing dye concentration. ZnO nanoparticles usually have a large surface area with lots of active sites for adsorption, especially when they are made from natural materials like *Laurus nobilis* leaves. When the concentration of the dye is reduced, a greater quantity of these active sites becomes accessible in proportion to the number of dye molecules. This results in a high percentage of dye removal, as each dye molecule has an ample number of sites to adhere to. When the concentration of the dye is reduced, a greater quantity of these active sites becomes accessible in proportion to the number of dye molecules. This results in a high percentage of dye removal, as each dye molecule has an ample number of sites to adhere to.

Effect of Adsorbent dosage on Adsorption efficiency

The MB removal efficiency as dependent on the adsorbent dosage is shown in Fig 6. In investigating this effect, the pH and dye concentration was fixed at 6 and 20 mg/L respectively to eliminate co-founding variables. The result shows that the maximum removal efficiency is retrieved at the 0.25 mg of adsorbent. The trend shows an increase in the dye removal with more adsorbent in the mixture. Several studies corroborate this finding, while some works show a stable dye adsorption percentage when the adsorbent amount increases. This phenomenon can be attributed to the increase in active sites, surface area and adsorption dynamics when adsorbent material increases.

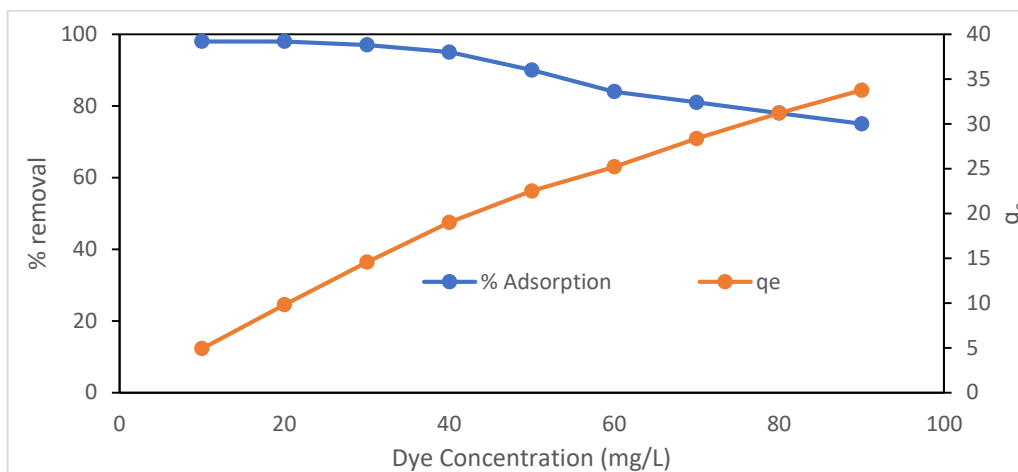


Fig. 5: Effect of Dye Concentration on dye removal.

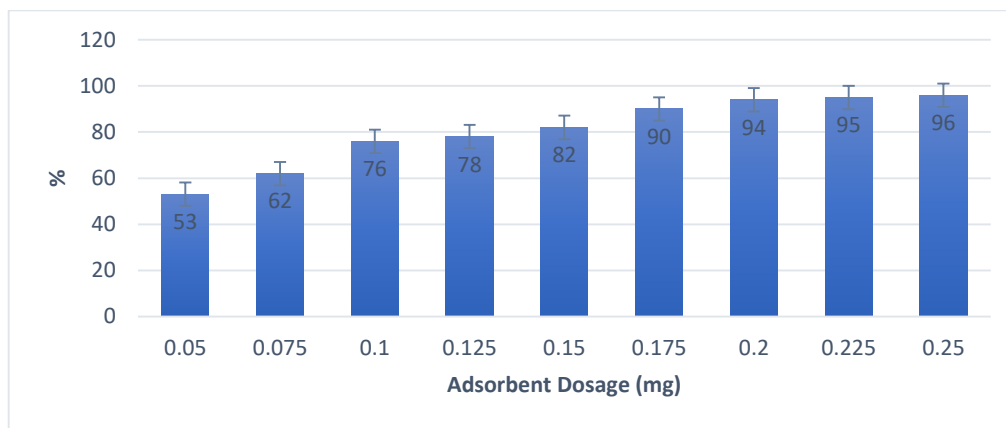


Fig. 6: Adsorbent dosage on MB removal efficiency.

Effect of pH on Adsorption Efficiency

The effect of solution pH on the adsorption efficiency was measured by varying the pH between 2 and 10. The other experimental variables of initial dye concentration, contact time, stirring speed, and adsorbent dosage were kept constant at 20 mg/L, 60 mins, 200 rpm and 0.2 g/L respectively. The analysis was also carried out at room temperature. We see from the result as displayed in Fig 7 that the adsorption efficiency (represented by the removal percent) was rather fairly constant at pH of 2-4. However, a significant reduction was seen from pH of 6-10. Because the surface hydroxyl groups have been protonated, ZnO nanoparticles are likely to have a positively charged surface at lower pH values (2-4). If the molecules of the dye, such as Methylene Blue, are anionic, which means they have a negative charge, then they will be strongly attracted to the positively charged surface of ZnO, which will result in effective adsorption. Under acidic conditions (lower pH), the dye molecules may exist in a state where adsorption onto the ZnO surface is more facile. At a reduced pH, the charge and chemical structure of the dye molecules may be more favourable for adsorption. Deprotonation results in the surface of ZnO becoming negatively charged as the pH rises (6-10). This weakens the electrostatic pull between the colour molecules and the material that absorbs them. Electrostatic repulsion may ensue if the pigment molecules are negatively charged within this pH range, thereby diminishing the efficacy of the adsorption process.

Effect of Contact Time on Adsorption Efficiency

Fig. 8 shows the effect of the contact time on the adsorption efficiency. The range of contact time was between 10 and 150 minutes. The other experimental variables of initial dye concentration, pH, stirring speed, and adsorbent dosage were kept constant at 20 mg/L, 6, 200 rpm, and 0.2 g/L respectively. The result shows a very step increase in the adsorption efficiency when the contact time

increases at the earlier stage (between 10 and 40 minutes). The reason for this is that at first, the adsorbent, such as ZnO, possesses a substantial quantity of accessible active sites. Due to the vacant nature of these sites, pigment molecules adhere to them rapidly, resulting in an exponential increase in adsorption. A significant concentration gradient exists between the dye in solution and the dye present on the surface of the adsorbent, which facilitates rapid adsorption. This behaviour is common during the beginning stages of adsorption processes. This increasing trend continues between 40 and 120 minutes though with lesser steepness. This can be attributed to the fact that as the number of dye molecules adsorbed onto the ZnO surface increases, there is a corresponding decrease in the concentration gradient, which serves as the propelling force for adsorption. This results in a deceleration of the rate of adsorption. A considerable proportion of the active sites becomes occupied, thereby posing a growing challenge for novel pigment molecules to locate accessible sites. The process continues albeit at a reduced pace. We also see that the removal percentage reduced at 150 minutes. This can be explained as that the active sites of the adsorbent become completely or nearly completely saturated with pigment molecules beyond a certain threshold. The saturation point restricts the capacity for further pigment adsorption. An equilibrium may be achieved in which the rate of adsorption is equivalent to the rate of desorption (dye molecules are released back into the solution), resulting in a net reduction or stabilisation of the removal percentage. Physical alterations such as adsorbent particle aggregation may transpire over time, diminishing the effective surface area and, consequently, the adsorption efficiency.

The obtained maximum adsorption is compared with similar studies in literature which investigated the adsorption of MB dye. We see that the result in this study is comparable to that obtained by several researchers (Table 2).

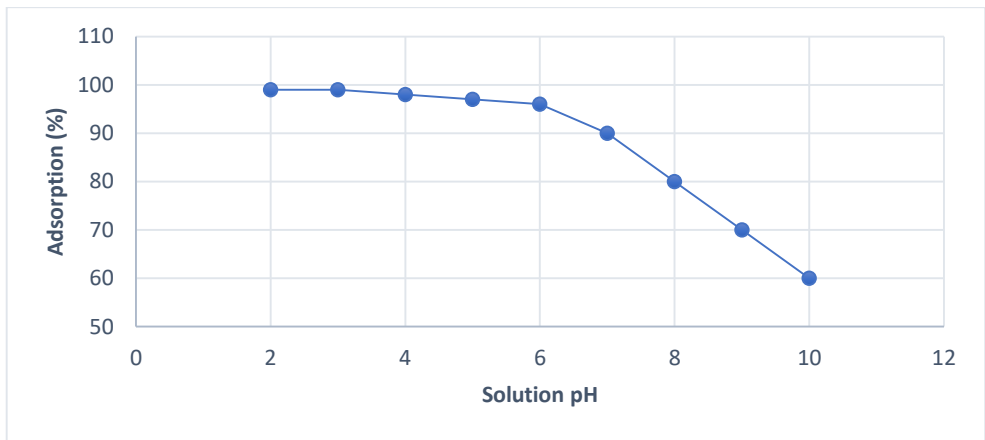


Fig. 7: Effect of Solution pH on the adsorption efficiency.

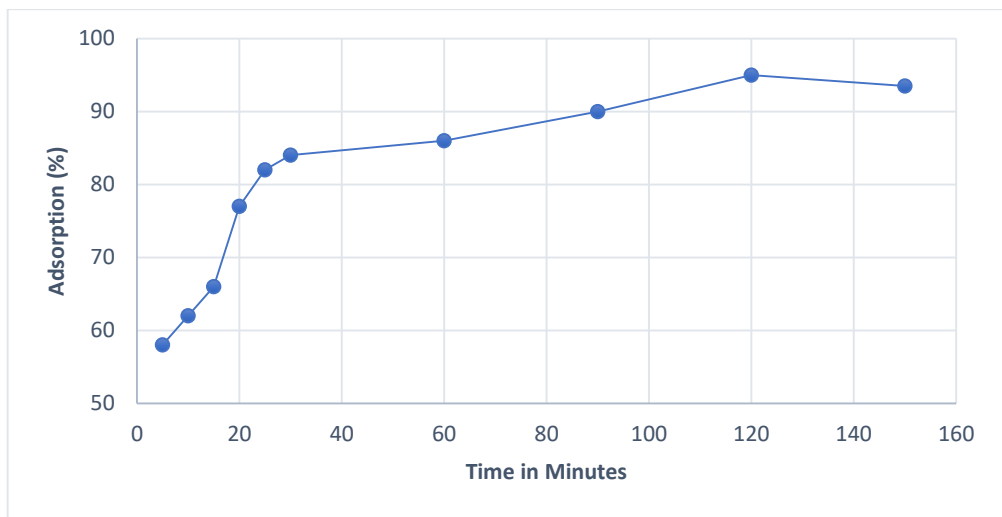


Fig 8: Effect of Contact time on the adsorption efficiency.

Table-2: Comparison of results of adsorption efficiency and optimal conditions for MB removal.

Adsorbents	Q _{max} (mg/g)	Removal percentage	Optimum conditions	Reference
Humic acid-coated Fe ₃ O ₄ nanoparticles	67.34	-	pH=11	[29]
microwave modified nano-silica (MW-nSiO ₂)	679.9	80%	Adsorbent dosage=100 mg/L, pH=6	[30]
ZnO	870.77	-	Insignificant	[31]
Ho-CaWO ₄ nanoparticles	103.09	71.17%	pH=2.03, contact time=15.16 min, adsorbent dose=1.91 g/L, and MB concentration =100.65 mg/L	[32]
EDTA-Silane functionalised CuO	-	54%	-	[33]
CuO	-	24%	-	[33]
a-chitin nanoparticles (CNP) prepared from Penaeus monodon shell waste	-	95%	pH=6, MB concentration =6 mg/L, contact time=30 min	[34]
	33.73	99%	pH=3, contact time 150=minutes, MB concentration =10 mg/L, adsorbent dose=0.25 mg/mL,	This Study

Adsorption Kinetics

Fig 9 shows the adsorption kinetics of the adsorption of the MB dye by the ZnO nanoparticle. We see that there was significant adsorption in the beginning periods of the process, as shown by the steep line. This adsorption slows down afterwards. The first and second-order pseudo equations are calculated in this work showing the reaction between the rate of chemical reaction and the reactant's concentration. This is used to describe the kinetics of the pollutant adsorption. The equation explains this mathematically:

$$\frac{dQ_t}{dt} = K(Q_{eq} - Q_t)^2 \tag{3}$$

where the amount of the MB dye is represented at a time t. The k is the second-order rate constant. The R² value for the first and second order is 0.704 and 0.904 respectively. The calculated q_{e,cal} and the experimental q_{e,exp} which represent the equilibrium adsorption capacity are 17.57 and 18.7 respectively.

The higher R² value of the Pseudo-second-order model shows a better/more accurate fit for the data as against the first-order model for the same data set. This is interpreted as the pseudo-second-order model describes more accurately the adsorption kinetics of the system, which is often the case in adsorption processes. This is corroborated in literature where the rate of occupying the adsorption sites is

proportional to the square of the number of unoccupied sites. Also, Table 3 shows that the experimental value (Q_e) is closer to the kinetic model for the Pseudo-Second-Order model.

Table-3: Adsorption Kinetics parameters of the MB dye onto green synthesized ZnO.

	Q _{e,exp} (mg/g)	Q _{e,cal.} (mg/g)	Absolute Difference (mg/g)	k (g/mg min)	R ²
Pseudo- first- Order	18.7	17.57	1.43	0.1341	0.7043
Pseudo- Second- Order	18.7	18.94	0.061	0.0121	0.9048

The difference between the experimental and the calculated values can be attributed to several factors. The experimental value is derived from actual adsorption experiments, which can be influenced by specific conditions such as temperature, pH, and stirring rate. These conditions might not be perfectly replicated in the theoretical model, leading to deviations. Additionally, the ZnO nanoparticles used in the experiments may possess unique surface characteristics, such as high surface area and active sites, which enhance adsorption beyond what is predicted by the model. Variations in the synthesis and preparation of the ZnO nanoparticles can result in differences in surface morphology and chemistry, affecting their adsorption capacity.

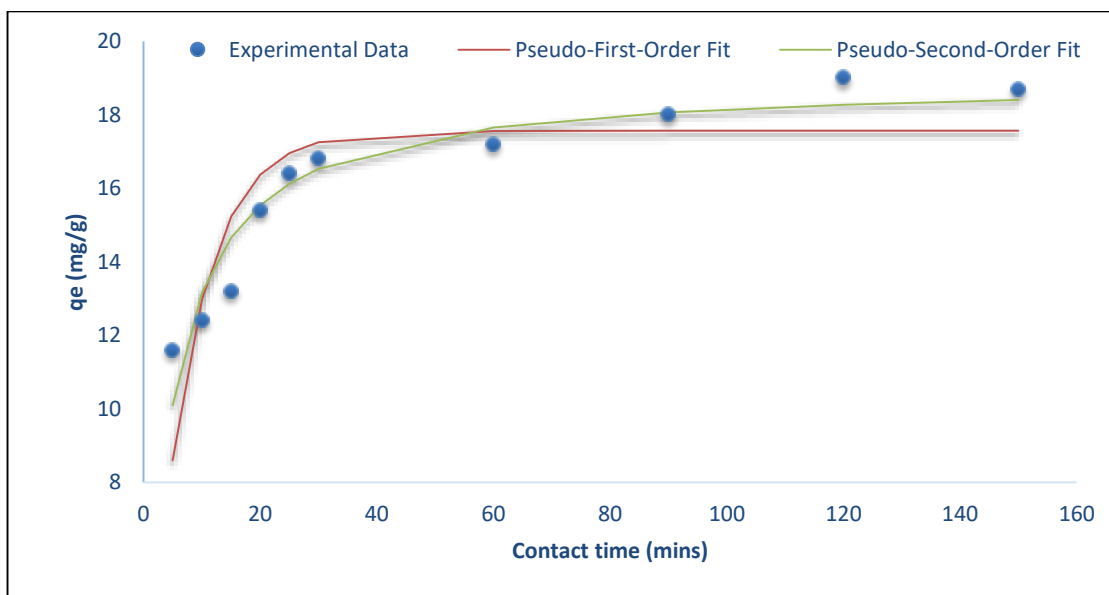


Fig 9: Effect of Contact time on adsorption of the MB dye on the ZnO adsorbent.

Another factor to consider is the presence of potential experimental errors and uncertainties. During the adsorption process, minor deviations in measurement, handling, or sample preparation can lead to discrepancies between the experimental and calculated values. These deviations, although usually minimal, can still impact the observed adsorption capacity.

Table-4: Langmuir and Freundlich equations for Adsorption Isotherm parameters for the MB Dye on ZnO adsorbent.

Langmuir $Q_{eq} = \frac{K_L Q_{max} C_{eq}}{1 + K_L C_{eq}}$			Freundlich $Q_{eq} = K_F C_{eq}^n$		
Q_{max} (mg/g)	K_L	R^2	n	K_F	R^2
30.98	1.027	0.9421	2.86	12.13	0.9463

Furthermore, the pseudo-second-order kinetic model, while generally providing a good fit for adsorption data, may not capture all the complexities of the adsorption process. The actual adsorption process might involve additional interactions and mechanisms that are not fully accounted for in the model. This can result in differences between the calculated and experimental equilibrium adsorption capacities. The higher experimental compared to the calculated is likely due to a combination of unique surface properties of the ZnO nanoparticles, specific experimental conditions, and potential experimental uncertainties. Despite these differences, the pseudo-

second-order model still provides a reasonably accurate description of the adsorption kinetics, as indicated by the high R^2 value and the close agreement between the experimental and calculated values.

Adsorption Isotherms

The Langmuir and Freundlich adsorption equations were used in quantitatively describing the adsorption of the MB dye on the ZnO Adsorbent. Equations 4 and 5 are used in representing the linear form of the isotherms, and Table-4 shows their equations and results.

$$\frac{C_{eq}}{Q_{eq}} = \frac{1}{Q_{max}} C_{eq} + \frac{1}{Q_{max} K_L} \tag{5}$$

$$\log Q_{eq} = \log K_F + n \log C_{eq} \tag{6}$$

where the maximum adsorbent capacity, Langmuir, and Freundlich adsorption constants are represented by Q_{max} (mg/g), K_L , and K_F respectively. The Freundlich exponential coefficient is shown as n . The slope and the intercept of Fig 10 represent the isotherms parameters for the MB adsorption. We see that for both the Langmuir and Freundlich adsorption models, the R^2 value was above 0.94, which indicates that there is an accurate fit of the experimental data by the models.

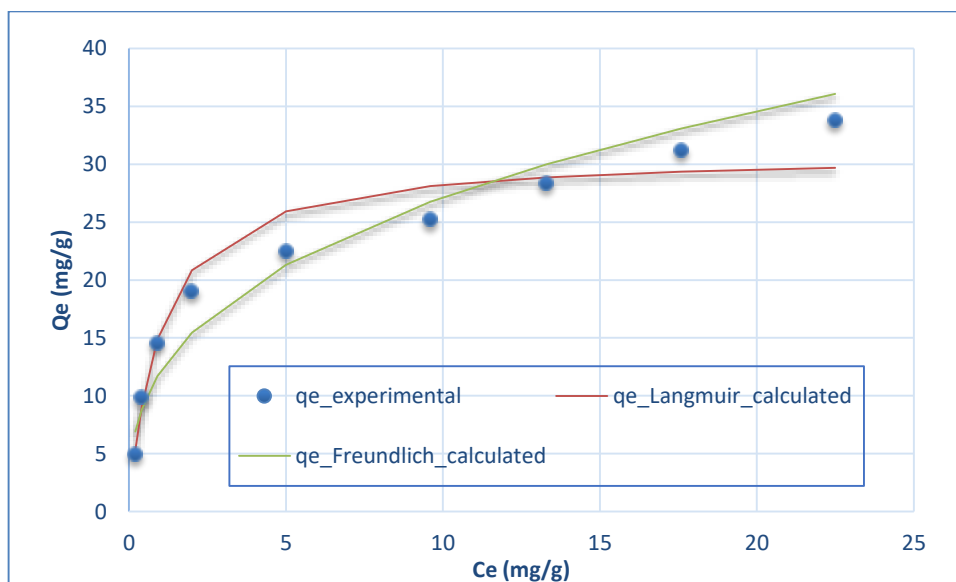


Fig. 10: Langmuir, and Freundlich adsorption isotherms.

Conclusion

The disposal of untreated water containing dyes poses significant risks to the environment and human health, particularly in aquatic ecosystems. MB, a commonly used dye in the textile industry, is known for its toxicity, mutagenicity, and persistence in water bodies. Nanoparticles, due to their high surface area-to-volume ratio, enhanced reactivity, and tunable surface functionalities, offer a promising solution for dye removal from wastewater.

In this study, we synthesized ZnO nanoparticles using a green synthesis method from *Laurus nobilis* leaf extract and zinc acetate dihydrate as the metal precursor. The synthesized ZnO nanoparticles were characterized using XRD, SEM, and FTIR. The nanoparticles were found to be monodispersed with an average size of 68.5 nm, exhibiting excellent morphological properties and high crystallinity.

The adsorption efficiency of the ZnO nanoparticles was tested under various experimental conditions, including pH, stirring time, adsorbent dosage, initial dye concentration, and contact time. The results demonstrated that the green synthesized ZnO nanoparticles effectively removed MB dye from water, achieving a maximum dye removal efficiency of 99% under optimal conditions of pH 3 and a contact time of 150 minutes. The maximum adsorption capacity of the ZnO nanoparticles for MB was determined to be 33.75 mg/g.

The adsorption kinetics were best described by the pseudo-second-order model, indicating that the rate of dye adsorption is proportional to the square of the number of unoccupied sites. This model provided a better fit for the experimental data compared to the first-order model, with R^2 values of 0.904 and 0.704, respectively. Additionally, the equilibrium adsorption capacity values, both experimental (18.7 mg/g) and calculated (17.57 mg/g), were in close agreement, further validating the pseudo-second-order model's accuracy.

The adsorption isotherms were analyzed using both the Langmuir and Freundlich models, with R^2 values above 0.94, indicating a good fit for the experimental data. The Langmuir model suggested a monolayer adsorption capacity of 30.98 mg/g, while the Freundlich model provided insights into the adsorption process on a heterogeneous surface.

Based on these observations and supported by established data and prior research, it can be

concluded that the green synthesized ZnO nanoparticles from *Laurus nobilis* leaf exhibit strong potential as an effective and environmentally friendly adsorbent for the removal of MB dye from contaminated water. Further studies should explore the adsorption capabilities of these nanoparticles on both cationic and anionic dyes to fully understand their functionality. Additionally, an economic analysis comparing green synthesized ZnO with chemically prepared ZnO could provide insights into the scalability and cost-effectiveness of this green synthesis approach.

References

1. A. Tkaczyk, K. Mitrowska, and A. Posyniak, Synthetic organic dyes as contaminants of the aquatic environment and their implications for ecosystems: A review, *Sci. Total Environ.*, **717**, 137222 (2020).
2. O. O. Alegbeleye, B. O. Opeolu, and V. A. Jackson, Polycyclic Aromatic Hydrocarbons: A Critical Review of Environmental Occurrence and Bioremediation, *Environ. Manage.*, **60**, 758 (2017).
3. A. Giwa *et al.*, Recent advances in advanced oxidation processes for removal of contaminants from water: A comprehensive review, *Process Saf. Environ. Prot.*, **146**, 220 (2021).
4. H. Basalius *et al.*, Green synthesis of nano-silver using *Syzygium samarangense* flower extract for multifaceted applications in biomedical and photocatalytic degradation of methylene blue, *Appl. Nanosci.*, **13**, 6, 3735 (2023).
5. I. Khan, I., Saeed, K., Zekker, I., Zhang, B., Hendi, A. H., Ahmad, A. & Khan, Review on methylene blue: Its properties, uses, toxicity and photodegradation., *Water*, **14**, 242 (2022).
6. C. N. C. Hasnam, Decolourisation and COD Reduction of Methylene Blue and Dye Wastewater Using *Sphingomonas Paucimobilis*, *THESIS*, 2013.
7. V. Katheresan, J. Kansedo and S. Y. Lau, Efficiency of various recent wastewater dye removal methods: A review, *J. Environ. Chem. Eng.*, **6**, 4676 (2018).
8. T. A. Kurniawan *et al.*, Functionalizing TiO₂ with graphene oxide for enhancing photocatalytic degradation of methylene blue (MB) in contaminated wastewater, *J. Environ. Manage.*, **270** (2020).
9. F. Mashkooor and A. Nasar, Magsorbents: Potential candidates in wastewater treatment technology – A review on the removal of methylene blue dye, *J. Magn. Magn. Mater.*, **500**, 166408 (2020).

10. Y. Zhou, J. Lu, Y. Zhou, and Y. Liu, Recent advances for dyes removal using novel adsorbents: A review, *Environ. Pollut.*, **252**, 352 (2019).
11. G. Crini, Non-conventional low-cost adsorbents for dye removal: A review, *Bioresour. Technol.*, **97**, 1061 (2006).
12. P. S. Goh, H. S. Kang, A. F. Ismail, W. H. Khor, L. K. Quen, and D. Higgins, Nanomaterials for microplastic remediation from aquatic environment: Why nano matters?, *Chemosphere*, **299**, 134418 (2022).
13. S. F. Ahmed *et al.*, "Nanomaterials as a sustainable choice for treating wastewater," *Environ. Res.*, **214**, 113807 (2022).
14. M. P. Ajith, M. Aswathi, E. Priyadarshini, and P. Rajamani, Recent innovations of nanotechnology in water treatment: A comprehensive review, *Bioresour. Technol.*, **342**, 126000 (2021).
15. A. Nayak, J. K. Sahoo, S. K. Sahoo, and D. Sahu, Removal of congo red dye from aqueous solution using zinc oxide nanoparticles synthesised from *Ocimum sanctum* (Tulsi leaf): a green approach, *Int. J. Environ. Anal. Chem.*, **102**, 7889 (2022).
16. T. P. M. Chu *et al.*, Synthesis, characterization, and modification of alumina nanoparticles for cationic dye removal, *Materials (Basel)*, **12**, 1 (2019).
17. N. M. Mahmoodi, Magnetic ferrite nanoparticle-alginate composite: Synthesis, characterization and binary system dye removal, *J. Taiwan Inst. Chem. Eng.*, **44**, 322 (2013).
18. S. Joshi, V. K. Garg, N. Kataria, and K. Kadirvelu, Applications of Fe₃O₄@AC nanoparticles for dye removal from simulated wastewater, *Chemosphere*, **236**, 124280 (2019).
19. F. Zhang, X. Chen, F. Wu, and Y. Ji, High adsorption capability and selectivity of ZnO nanoparticles for dye removal, *Colloids Surfaces A Physicochem. Eng. Asp.*, **509**, 474 (2016).
20. F. T. Thema, E. Manikandan, M. S. Dhramini, and M. Maaza, Green synthesis of ZnO nanoparticles via *Agathosma betulina* natural extract," *Mater. Lett.*, **161**, 124 (2015).
21. M. Ramesh, M. Anbuvaran, and G. Viruthagiri, Green synthesis of ZnO nanoparticles using *Solanum nigrum* leaf extract and their antibacterial activity, *Spectrochim. Acta - Part A Mol. Biomol. Spectrosc.*, **136**, 864 (2015).
22. C. A. Soto-Robles *et al.*, Study on the effect of the concentration of *Hibiscus sabdariffa* extract on the green synthesis of ZnO nanoparticles, *Results Phys.*, **15** (2019).
23. Z. Al-Qodah, W. K. Lafi, Z. Al-Anber, M. Al-Shannag, and A. Harahsheh, Adsorption of methylene blue by acid and heat treated diatomaceous silica, *Desalination*, **217**, 212 (2007)
24. L. Fu and Z. Fu, Plectranthus amboinicus leaf extract-assisted biosynthesis of ZnO nanoparticles and their photocatalytic activity, *Ceram. Int.*, **41**, 2492 (2015).
25. H. M. H. Al-Kordy, S. A. Sabry, and M. E. M. Mabrouk, Statistical optimization of experimental parameters for extracellular synthesis of zinc oxide nanoparticles by a novel haloaliphilic *Alkalibacillus* sp.W7, *Sci. Rep.*, **11**, 1 (2021).
26. Z. Es'haghi, M. Mohammadian, and S. Hooshmand, Green and chemical synthesis of zinc oxide nanoparticles and size evaluation by UV-vis spectroscopy, *J. Nanomedicine Res.*, **7**, 52 (2018).
27. S. Vijayakumar, B. Vaseeharan, B. Malaikozhundan, and M. Shobiya, *Laurus nobilis* leaf extract mediated green synthesis of ZnO nanoparticles: Characterization and biomedical applications, *Biomed. Pharmacother.*, **84**, 1213 (2016).
28. H. Garbacz, Biological properties, *Nanocrystalline Titan.*, **175** (2018).
29. X. Zhang, P. Zhang, Z. Wu, L. Zhang, G. Zeng, and C. Zhou, Adsorption of methylene blue onto humic acid-coated Fe₃O₄ nanoparticles, *Colloids Surfaces A Physicochem. Eng. Asp.*, **435**, 85 (2013)
30. E. C. Peres, J. C. Slaviero, A. M. Cunha, A. Hosseini-Bandegharaci, and G. L. Dotto, Microwave synthesis of silica nanoparticles and its application for methylene blue adsorption, *J. Environ. Chem. Eng.*, **6**, 649 (2018).
31. F. Zhang, J. Lan, Y. Yang, T. Wei, R. Tan, and W. Song, Adsorption behavior and mechanism of methyl blue on zinc oxide nanoparticles, *J. Nanoparticle Res.*, **15**, 11 (2013)
32. C. A. Igwegbe *et al.*, Modeling of adsorption of Methylene Blue dye on Ho-CaWO₄ nanoparticles using Response Surface Methodology (RSM) and Artificial Neural Network (ANN) techniques, *MethodsX*, **6**, 1779 (2019).
33. M. P. Geetha, P. Pratheeksha, and B. K. Subrahmanya, Development of functionalized CuO nanoparticles for enhancing the adsorption of methylene blue dye, *Cogent Eng.*, **7**, 1 (2020).
34. S. Dhananasekaran, R. Palanivel, and S. Pappu, Adsorption of Methylene Blue, Bromophenol Blue, and Coomassie Brilliant Blue by α -chitin nanoparticles, *J. Adv. Res.*, **7**, 113 (2016).